

See discussions, stats, and author profiles for this publication at: <https://www.researchgate.net/publication/231701821>

# Computational Studies on Isospecific Polymerization of 1-Hexene Catalyzed by Cationic Rare Earth Metal Alkyl Complex Bearing a C<sub>3</sub>iPr-trisox Ligand

ARTICLE *in* MACROMOLECULES · JANUARY 2012

Impact Factor: 5.8 · DOI: 10.1021/ma202414k

---

CITATIONS

13

---

READS

14

## 6 AUTHORS, INCLUDING:



**Yi Luo**

118 PUBLICATIONS 1,751 CITATIONS

[SEE PROFILE](#)

## Computational Studies on Isospecific Polymerization of 1-Hexene Catalyzed by Cationic Rare Earth Metal Alkyl Complex Bearing a $C_3$ iPr-trisox Ligand

Xiaohui Kang,<sup>†</sup> Yuming Song,<sup>†</sup> Yi Luo,<sup>\*,†</sup> Gang Li,<sup>‡</sup> Zhaomin Hou,<sup>\*,†,§</sup> and Jingping Qu<sup>\*,†</sup>

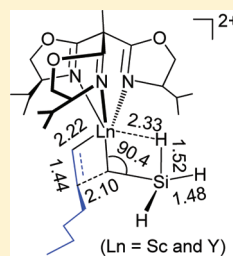
<sup>†</sup>State Key Laboratory of Fine Chemicals, School of Pharmaceutical Science and Technology, Dalian University of Technology, Dalian 116024, China

<sup>‡</sup>School of Chemical Engineering, Dalian University of Technology, Dalian 116024, China

<sup>§</sup>Organometallic Chemistry Laboratory, RIKEN Advanced Science Institute, 2-1 Hirosawa, Wako, Saitama 351-0198, Japan

### Supporting Information

**ABSTRACT:** 1-Hexene polymerization catalyzed by dicationic rare earth metal alkyl species  $[\text{Ln}(\text{iPr-trisox})(\text{CH}_2\text{SiMe}_3)]^{2+}$  ( $\text{Ln} = \text{Sc}$  and  $\text{Y}$ ; trisox = trisoxazoline) has been computationally studied by using QM/MM approach. It has been found that the initiation of 1-hexene polymerization kinetically prefers 1,2-insertion (free energy barrier of 17.23 kcal/mol) to 2,1-insertion (free energy barrier of 20.05 kcal/mol). Such a preference of 1,2-insertion has been also found for chain propagation stage. The isotactic polymerization was computed to be more kinetically preferable in comparison with syndiotactic manner, and the dicationic system resulted in lower insertion free energy barrier and more stable insertion product in comparison with the monocationic system. The stereoselectivity was found to follow chain-end mechanism, and the isospecific insertion of 1-hexene is mainly controlled by kinetics. In addition, the current computational results, for the first time, indicate that the higher activity of Sc species toward 1-hexene polymerization in comparison with the Y analogue could be ascribed to lower insertion barrier, easier generation of the active species, and its larger chemical hardness.



### INTRODUCTION

Poly(1-hexene) as an important long-chain poly( $\alpha$ -olefin) is a pectinate polymer with special properties. It can be used as oil additive, which is suitable for lowering setting point, lowering dynamic viscosity, and limiting shear tension of paraffin oils under transportation and storage conditions. Generally, the microstructure of synthetic polymer has significant influences on its physical and chemical properties, and hence for certain usage. Therefore, the synthesis of poly(1-hexene) with certain microstructure has attracted more and more interests. In this context, group 4 and late transition metal complexes have been widely used as precatalysts.<sup>1,2</sup> For example, *ansa*-zirconium catalysts,<sup>2a</sup> zirconium and rhodium heterobimetallic complexes,<sup>2b</sup> and chiral  $[N,N,N]$ -ligated titanium/zirconium catalysts<sup>2c</sup> have been reported for 1-hexene polymerization. These catalysts have  $C_1$  or  $C_2$  symmetric feature and show excellent isospecific control in 1-hexene polymerization. However, catalyst systems showing both high activity and stereoselectivity for 1-hexene polymerization remained rare.<sup>2b,j</sup> The zirconium amine bis(phenoxide) complexes have been reported to be highly active precatalysts for 1-hexene polymerization, whereas the polymers obtained were atactic in spite of the  $C_1$  symmetric feature of the ancillary ligand.<sup>2d</sup> Kol and his co-workers reported a Ti diamine bis(phenolate) catalyst showing high activity toward 1-hexene polymerization, but the polymer obtained had low-to-medium degree of isospecificity.<sup>2e</sup> Therefore, studies on the search for highly active and stereoselective

catalysts for 1-hexene polymerization are of much interest and importance.

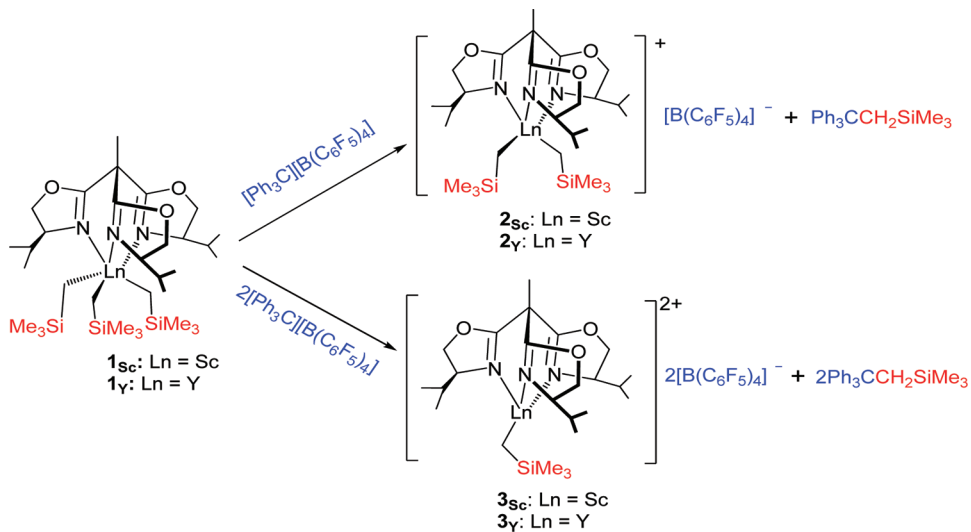
Recently, cationic rare earth alkyl complexes have been reported to act as a new family of polymerization catalysts.<sup>3</sup> For example, the cationic half-sandwich scandium alkyl species, such as  $[(C_5Me_4SiMe_3)Sc(CH_2SiMe_3)]^+$ , showed excellent activity and selectivity for the polymerization and copolymerization of a wide range of olefins, such as syndiospecific polymerization and copolymerization of styrene with ethylene, dienes and other olefins.<sup>4</sup> However, this catalyst showed no stereoselectivity for the polymerization of 1-hexene, yielding poly(1-hexene) in both 1,2- and 2,1-fashions.<sup>5</sup> The cationic scandium alkyl species bearing a neutral 1,4,7-trithiacyclonanone ligand,  $[Sc([9]aneS_3)(CH_2SiMe_3)]^+$ , was also reported to polymerize 1-hexene but without showing stereoselectivity.<sup>6</sup> Gade et al. reported that a series of cationic rare-earth metal alkyl species, such as those of  $2_{\text{Sc}}$  ( $2_{\text{Y}}$ ) and  $3_{\text{Sc}}$  ( $3_{\text{Y}}$ ) shown in Scheme 1, bearing a  $C_3$ -chiral trisoxazoline (trisox) ancillary ligand could be generated by the reaction of a trialkyl complex  $\text{Ln}(\text{iPr-trisox})(\text{CH}_2\text{SiMe}_3)_3$ , such as  $1_{\text{Sc}}$  ( $1_{\text{Y}}$ ), with 1 and 2 equiv of a borate compound  $[\text{Ph}_3\text{C}][\text{B}(\text{C}_6\text{F}_5)_4]$  as an activator, respectively (Scheme 1).<sup>7</sup> Among these species, the dicationic Sc alkyl species showed extremely high activity ( $36200 \text{ kg mol}^{-1} \text{ h}^{-1}$ ) and isoselectivity toward the polymerization of 1-hexene.

Received: October 31, 2011

Revised: December 20, 2011

Published: January 9, 2012



**Scheme 1.** Generation of Cationic Rare Earth Metal Alkyl Species Bearing  $C_3$ -Chiral Trisoxazoline Ancillary Ligand

However, other dicationic rare-earth metal alkyl species showed rather low or no activity,<sup>7c</sup> and all of the monocationic species showed lower activity in comparison with their corresponding dicationic analogues. However, the related mechanism and factors governing the activity and regio- and stereoselectivity remain unclear.

Numerous computational studies<sup>8–11</sup> have been widely and successfully conducted to investigate the mechanism of various olefin polymerizations catalyzed by group 4 and late transition metal complexes. In this context, studies on  $\alpha$ -alkenes have almost been limited to propylene possibly due to the bulky substituent of higher alkenes. A palladium-catalyzed polymerization of propylene has been computationally explored.<sup>10a</sup> It was found that 2,1-insertion is more favorable than 1,2-insertion in the palladium catalyst system, and the insertion barrier of propylene was higher than that of ethylene. However, the polymerization of propylene catalyzed by a series of Ti complexes featuring fluorine-containing phenoxy-imine chelate ligands was computationally found to occur exclusively via 1,2-insertion at the initial stage and 2,1-insertion as the principal mode in the chain propagation.<sup>10h</sup> Caporaso et al. reported a more general picture of the enantioselectivity in the process of chain transfer to monomer during propylene polymerization.<sup>10l</sup>

In comparison with computational studies on the polymerization of propylene and other olefins, the polymerization 1-hexene has received much less attention.<sup>8</sup> Carpentier et al. optimized a variety of possible cationic zirconium species, which was used in the stereospecific polymerization of 1-hexene.<sup>11a</sup> The first determination of empirical and computed <sup>12</sup>C/<sup>13</sup>C kinetic isotope effects for metallocene-catalyzed polymerization of propylene as a model of the 1-hexene was also reported.<sup>11b</sup> Thomson and co-workers studied the quantitative effects of ion pair and sterics on chain propagation kinetics in 1-hexene polymerization catalyzed by mixed Cp'/ArO ligated complexes.<sup>11d</sup> They found that the Ti-based catalyst exhibiting unusually high reactivity has lower ion-pair separation energy in toluene in comparison with the Zr analogue. Extensive theoretical studies on the mechanism of olefin polymerization by late and group 4 transition metal complexes effectively promoted the design and development of homogeneous transition metal catalyst.

In contrast, computational studies on the mechanism of olefin polymerization catalyzed by rare-earth metal catalysts have been much less explored despite recent progress.<sup>12,13</sup> Recently, Maron

et al. conducted a series of computational studies on the syndiospecific polymerization of styrene by single-component ansa-lanthanidocenes,<sup>12l,n</sup> the polymerization of conjugated dienes by cationic species  $[Cp^*ScR]^+$ , and the copolymerization of conjugated dienes with olefins (including 1-hexene) by a hemilanthanidocene  $[(Cp^*)(BH_4)LnR]$ .<sup>12k,m</sup> A computational study on styrene polymerization catalyzed by *ansa*-bis(indenyl) allyl rare earth complexes was reported by Carpentier and co-workers. The results suggested a favorable secondary insertion of styrene during both chain initiation and propagation stages.<sup>12o</sup> Mountford et al. performed a DFT study on the ligand binding ability in  $Ln(L)(CH_2SiMe_3)_3$  ( $Ln = Sc$  or  $Y$ ;  $R = Me$  or  $CH_2SiMe_3$ ;  $L = Me_3[9]aneN_3$  or  $[9]aneS_3$ ) complexes. They found that the electron-deficient base-free dialkyl cations  $[Ln(L)(CH_2SiMe_3)_2]^+$  were usually stabilized by a  $\beta$ -Si–C agostic interaction.<sup>12a</sup> During our computational studies on rare earth metal complexes,<sup>13</sup> we have also carried out a series of theoretical calculations on olefin polymerization catalyzed by cationic rare earth metal complexes in combination with experimental studies.<sup>12b–e</sup> We recently found that the mechanism of styrene–ethylene copolymerization catalyzed by a cationic half-sandwich scandium alkyl species is different from that involved in group 4 catalyst systems.<sup>12f</sup> In spite of these recent achievements in this field, an in-depth study on 1-hexene polymerization catalyzed by a rare earth metal catalyst has not been reported previously.

In this paper, we report a QM/MM (quantum mechanics/molecular mechanics) study on the mechanism of 1-hexene polymerization catalyzed by the dicationic alkyl complex  $[Sc(iPr\text{-trisox})(CH_2SiMe_3)]^{2+}$ . The catalytic activity of this cationic species has also been computationally compared with its Y analogue. There are three purposes in this study. The first is to clarify whether the 1-hexene insertion preferably adopts a 1,2-insertion or 2,1-insertion manner in the chain initiation and propagation stages. The second is to find out the reason why such kind of catalyst system produced isotactic poly(1-hexene). The third is to computationally clarify the origins of the higher activity of dicationic active species in comparison with the monocationic ones and the higher activity of Sc species compared to Y analogue. We hope that the results reported here would be helpful for better understanding of the polymerization

mechanism of 1-hexene and for the development of new rare-earth metal polymerization catalysts.

## ■ COMPUTATIONAL DETAILS

The dicationic scandium alkyl species  $[\text{Sc}(i\text{Pr}-\text{trisoxy})(\text{CH}_2\text{SiH}_3)]^{2+}(3_{\text{Sc}}')$  (Figure 1) was used for modeling the initial

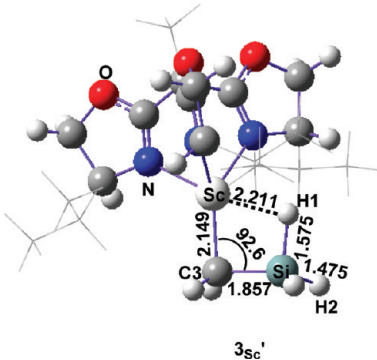


**Figure 1.** Optimized cationic species  $3_{\text{Sc}}'$  showing a  $\beta$ -Si–H agostic interaction as suggested by the  $\text{Sc}\cdots\text{H}$  distance of 2.211 Å, Si–H1 bond length of 1.575 Å, and  $\text{Sc}\cdots\text{C3}\cdots\text{Si}$  angle of 92.6°. The similar geometrical feature, viz.  $\beta$ -Si–C agostic interaction, was also observed in real structure  $[\text{Sc}(i\text{Pr}-\text{trisoxy})(\text{CH}_2\text{SiMe}_3)]^{2+}$  ( $3_{\text{Sc}}$ , see Figure S-3 in Supporting Information).

catalytic species in the computations. The QM/MM calculations were carried out with ONIOM(B3LYP:UFF) approach,<sup>14</sup> as implanted in Gaussian 09 program.<sup>15</sup> In the ONIOM(B3LYP:UFF) calculations, one methyl and three isopropyl groups of the ancillary ligand are placed in the outside layer treated by the universe force field (UFF)<sup>16</sup> for saving computational time and consideration of steric effects. The other atoms, including those in the monomer molecules, constitute the inner layer. During the calculations on the generation of ion pair and its separation, the species  $[\text{Ln}(i\text{Pr}-\text{trisoxy})(\text{CH}_2\text{SiMe}_3)]^{2+}$  ( $\text{Ln} = \text{Sc}$  and  $\text{Y}$ ) and counterion  $[\text{B}(\text{C}_6\text{F}_5)_4]$  were adopted. The ONIOM-(B3LYP:UFF) method was used for geometry optimization and subsequent analytic frequency calculation. The treatment of  $[\text{Ln}(i\text{Pr}-\text{trisoxy})(\text{CH}_2\text{SiMe}_3)]^{2+}$  species for the ONIOM calculation is same as that described above. As to the part of  $[\text{B}(\text{C}_6\text{F}_5)_4]$  anion, the B atom and the  $-\text{C}_6\text{F}_5$  group interacting directly with the metal atom are included in the inner layer. While the remained three  $-\text{C}_6\text{F}_5$  groups are placed in the outside layer. The ONIOM energy of the whole system is calculated as

$$E(\text{ONIOM}) = E(\text{high-level, inner layer}) + E(\text{low-level, real}) \\ - E(\text{low-level, inner layer})$$

where the  $E(\text{high-level, inner layer})$  is the energy of the inner layer calculated with the high-level method (B3LYP),  $E(\text{low-level, real})$  is the energy of the whole system calculated with the low-level method (UFF force field), and  $E(\text{low-level, inner layer})$  is the energy of the inner layer calculated with the low-level method. For the B3LYP calculation, the 6-31G\* basis set was used for C, H, N, O, B, and F atoms, and the Sc, Y and Si atoms were treated by the Stuttgart/Dresden effective core potential (ECP) and the associated basis sets.<sup>17</sup> In the Stuttgart/Dresden ECP used in this study, the most inner 10 electrons of Si and Sc and the most inner 28 electrons of Y are included in the core, respectively. The 4 valence electrons of Si atom and 11 valence electrons of Sc and Y atoms were treated by the optimized basis sets, viz.  $(4s4p)/[2s2p]$  for Si,  $(8s7p6d1f)/[6s5p3d1f]$  for Sc, and  $(8s7p6d)/[6s5p3d]$  for Y, respectively. The basis set for Sc atom contains one f-polarization function with exponent of 0.27. One f-polarization function (exponent of 0.84) and one d-polarization function (exponent of 0.45) were augmented for Y and Si, respectively. Normal-coordinate analyses were performed to

verify the geometrically optimized stationary points and to obtain the thermodynamic data. In the present study, the complexation energy was defined as the energy difference in free energy between a  $\pi$ -complex and separated species. The more negative the complexation energy, the more favorable the formation of a  $\pi$ -complex. Insertion barriers were calculated as the difference between the transition state and the most stable structures (separated species or  $\pi$ -complex). Reaction energies were calculated as the energy difference between the insertion product and the energy sum of isolated monomer and active species. All optimizations were carried out in the gas phase without any symmetry constraint. Energy profiles were described by relative free-energies obtained from gas-phase ONIOM calculations ( $\Delta G$ , kcal/mol).

The basis set superposition error (BSSE) correction was included in the calculation of interaction energy between the active species and 1-hexene motif. For estimation of BSSE, single point calculations were performed for the ONIOM-optimized geometries. To estimate the changes in enthalpy during the formation of ion pair and their separation via the coordination of olefin, single-point energy calculations were also performed on optimized ONIOM geometries. In such single-point calculations, the larger basis set 6-31+G\*\* was used for nonmetal atoms, and the basis sets for metal atoms are same as those in geometry optimizations. The enthalpy correction obtained from analytic frequency calculation was added to the single-point energy to estimate enthalpy change. Such single-point calculations were also performed for some structures to obtain chemical hardness.

## ■ RESULTS AND DISCUSSION

### 1. Regioselectivity in the Insertion Reaction of 1-Hexene.

For  $d^0$ -metal complex catalyst, the insertion reaction of alkenes was proposed to follow the Cossee–Arlman mechanism,<sup>18</sup> in which the olefin initially approaches the metal center to form a  $\pi$ -complex and then the reaction proceeds via a four-center transition state (TS) leading to the insertion product (Scheme 2a). This general mechanism is also suitable for hexene insertions into the  $\text{Sc}-\text{CH}_2\text{SiH}_3$  bond of  $3_{\text{Sc}}'$ . The hexene polymerization, however, has some differences from ethylene polymerization. Two C atoms of the ethylene are equivalent when inserting the metal–alkyl (M–R) bond, while the insertion of a hexene into the M–R bond can adopt two manners with two enantiofaces,<sup>19</sup> viz. 1,2-insertion (primary insertion with *re*- and *si*-faces in the transition state, respectively) and 2,1-insertion (secondary insertion with *re*- and *si*-faces in the transition state, respectively) because of the existence of an *n*-butyl group (Scheme 2b). Therefore, the issue of regioselectivity appears in the polymerization of an  $\alpha$ -olefin.

In the present paper, we investigated in detail the regioselectivity of 1-hexene polymerization. Considering that the regioselectivity is determined by an insertion TS structure, four TSs for the insertion of 1-hexene into  $\text{Sc}-\text{CH}_2\text{SiH}_3$  bond of  $3_{\text{Sc}}'$  have been located with respect to 1,2-*si*-, 1,2-*re*-, 2,1-*si*-, and 2,1-*re*-insertion manners, respectively. It was found that free energies (relative to the energy sum of  $3_{\text{Sc}}'$  and 1-hexene) of these TSs are 18.70, 19.51, 25.07, and 30.19 kcal/mol for 1,2-*si*-, 1,2-*re*-, 2,1-*si*-, and 2,1-*re*-insertion manners, respectively (see Figure S-4 in Supporting Information). This result indicates that the 1,2-*si*-insertion TS is most stable among these four TSs and that the 2,1-*si*-insertion TS is more stable than 2,1-*re*-insertion TS. Therefore, the 1,2-*si*-insertion pattern was considered in the following, and the 2,1-*si*-insertion manner was also investigated for comparison. The computed energy profiles for 1,2- and 2,1-insertion of 1-hexene into the  $\text{Sc}-\text{CH}_2\text{SiH}_3$  bond of  $3_{\text{Sc}}'$  are shown in Figure 2. As shown in this figure, the free energies are relative to the energy sum of active species  $3_{\text{Sc}}'$  and  $\mathbf{m}$  (monomer, 1-hexene). The 1,2-insertion starts with the formation of complex  $\mathbf{C}_{12\text{Sc}}$  and proceeds via a

**Scheme 2.** (a) Cossee–Arlman Mechanism for Alkene Insertion into a Metal–Alkyl Bond and (b) Four Possible Transition States for the Insertion of a Hexene into the M–R Bond

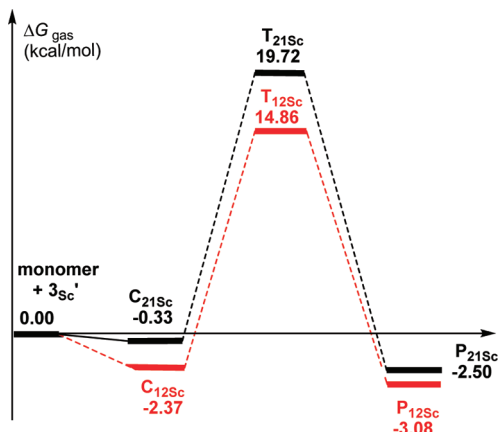
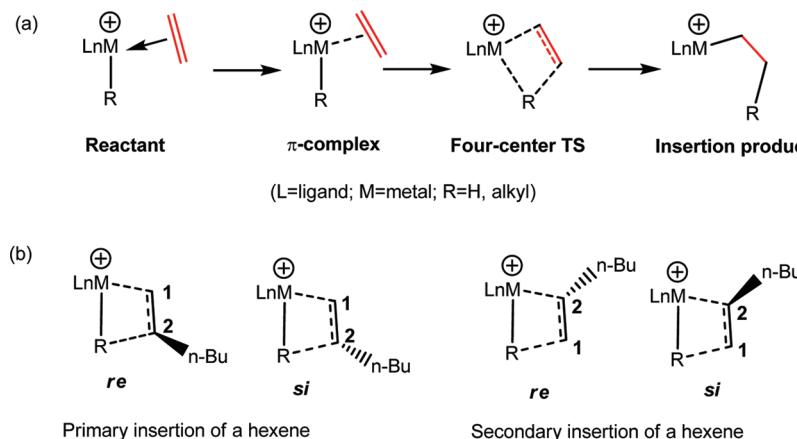


**Figure 2.** Computed energy profiles (energy in kcal/mol) for 1,2- and 2,1-insertion of 1-hexene at the chain initiation stage.

four-center transition state  $T_{12\text{Sc}}$ , leading to the insertion product  $P_{12\text{Sc}}$ . The  $C_{12\text{Sc}}$  is lower in free energy than the energy sum of  $3_{\text{Sc}}'$  and  $m$  by  $-2.37$  kcal/mol. This insertion process, which overcomes a free energy barrier of  $17.23$  kcal/mol, is exergonic by  $-3.08$  kcal/mol. However, the 2,1-insertion needs to overcome a free-energy barrier of  $20.05$  kcal/mol and is exergonic by  $-2.50$  kcal/mol. Both the prereaction complex ( $C_{21\text{Sc}}$ ) and transition state ( $T_{21\text{Sc}}$ ) for 2,1-insertion are higher in energy than those for 1,2-insertion by  $2.04$  and  $4.86$  kcal/mol, respectively. The 1,2-insertion product  $P_{12\text{Sc}}$  is also slightly stable than the 2,1-insertion product  $P_{21\text{Sc}}$ . Single-point calculations at the level of B3LYP were also performed on the optimized stationary points involved in Figure 2. In the single-point calculations, the basis set 6-311+G\*\* was used for C, H, O, and N atoms and the basis set for Sc and Si atoms are same as that in geometry optimizations. The results show that the insertion free energy barrier for 1,2-insertion is smaller than that for 2,1-insertion by  $6.12$  kcal/mol, and the  $P_{12\text{Sc}}$  is more stable than  $P_{21\text{Sc}}$  by  $3.39$  kcal/mol (see Figure S-1 in Supporting Information). To corroborate this result, the MPW1K functional has been also utilized to compute the energy profile. The MPW1K functional developed by Truhlar's group was suggested to be an efficient method for predicting reaction energy and barrier heights and was comparable to multi-reference methods.<sup>20</sup> The MPW1K calculations also indicate the preference of 1,2-insertion over 2,1 insertion (see Figure S-2

in Supporting Information). These results suggests that the 1,2-insertion is both kinetically and energetically more favorable than the 2,1-insertion at the chain initiation stage. To elucidate the origin of the kinetic preference for such a regioselectivity, we further analyzed the energies and geometries of  $T_{12\text{Sc}}$  and  $T_{21\text{Sc}}$ . An analysis of energy (electronic energy,  $\Delta E_{\text{TS}}$ ) decomposition of  $T_{12\text{Sc}}$  and  $T_{21\text{Sc}}$  was performed. The energies of the fragments  $\text{Sc}(i\text{Pr}-\text{trisox})(\text{CH}_2\text{SiH}_3)^{2+}$  (A) and 1-hexene (B) in the geometry they have in the two TSs were evaluated in single-point calculations. Such single-point energies of the fragments and the energy (corrected by BSSE) of TS were used to estimate the interaction energy  $\Delta E_{\text{int}}$ . These energies, together with the energy of the respective fragments in their optimal geometry, allow for the estimation of the deformation energies of the two fragments,  $\Delta E_{\text{def}}(\text{A})$  and  $\Delta E_{\text{def}}(\text{B})$ . As the energy of the TS,  $\Delta E_{\text{TS}}$ , is evaluated with respect to the energy of the two separated fragments, the relation  $\Delta E_{\text{TS}} = \Delta E_{\text{int}} + \Delta E_{\text{def}}(\text{A}) + \Delta E_{\text{def}}(\text{B})$  holds. The following components were found for  $T_{12\text{Sc}}$ :  $\Delta E_{\text{int}} = -37.21$  kcal/mol;  $\Delta E_{\text{def}}(\text{A}) = 18.83$  kcal/mol;  $\Delta E_{\text{def}}(\text{B}) = 25.10$  kcal/mol; and therefore  $\Delta E_{\text{TS}} = 6.72$  kcal/mol. While the following components were found for  $T_{21\text{Sc}}$ :  $\Delta E_{\text{int}} = -28.08$  kcal/mol;  $\Delta E_{\text{def}}(\text{A}) = 20.08$  kcal/mol;  $\Delta E_{\text{def}}(\text{B}) = 20.71$  kcal/mol; and therefore  $\Delta E_{\text{TS}} = 12.71$  kcal/mol. The  $\Delta E_{\text{TS}}$  value of  $12.71$  kcal/mol for  $T_{21\text{Sc}}$  is larger than that for  $T_{12\text{Sc}}$  by  $5.99$  kcal/mol. It is obvious that the total  $\Delta E_{\text{def}}$  of  $43.93$  kcal/mol in  $T_{12\text{Sc}}$  is larger than that ( $40.79$  kcal/mol) in  $T_{21\text{Sc}}$ . However, the increased deformation energy could be compensated by the favorable  $\Delta E_{\text{int}}$  ( $-37.21$  kcal/mol) in  $T_{12\text{Sc}}$  and resulted in lower  $\Delta E_{\text{TS}}$  ( $6.72$  kcal/mol) for  $T_{12\text{Sc}}$  in comparison with that ( $12.71$  kcal/mol) for  $T_{21\text{Sc}}$ . Therefore, the more favorable interaction of A with B in  $T_{12\text{Sc}}$  could account for more stability of  $T_{12\text{Sc}}$  in comparison with  $T_{21\text{Sc}}$ . Structurally, in  $T_{21\text{Sc}}$  (Figure 3), a repulsive interaction between the ancillary ligand and the  $\text{CH}_3(\text{CH}_2)_3$  group of 1-hexene moiety could exist, which destabilized  $T_{21\text{Sc}}$ , whereas such an interaction is absent in  $T_{12\text{Sc}}$ . The  $\text{C}1=\text{C}2$  bond length of 1-hexene moiety is  $1.440$  Å in  $T_{12\text{Sc}}$  and  $1.425$  Å in  $T_{21\text{Sc}}$ , suggesting that the  $\text{C}1=\text{C}2$  double bond was more activated in the former. The  $T_{12\text{Sc}}$  has a shorter  $\text{Sc}-\text{C}1$  (2.218 Å) bond length than the  $\text{Sc}-\text{C}2$  (2.268 Å) in  $T_{21\text{Sc}}$ , which suggests that the 1-hexene moiety interacts with the metal center more tightly in  $T_{12\text{Sc}}$  compared with  $T_{21\text{Sc}}$ . This is in line with the analysis of energy decomposition described above. The geometrical character associated with the  $\beta$ -Si–H agostic interactions in  $T_{12\text{Sc}}$  (2.331 Å for  $\text{Sc}\cdots\text{H}1$ , 1.524 Å for

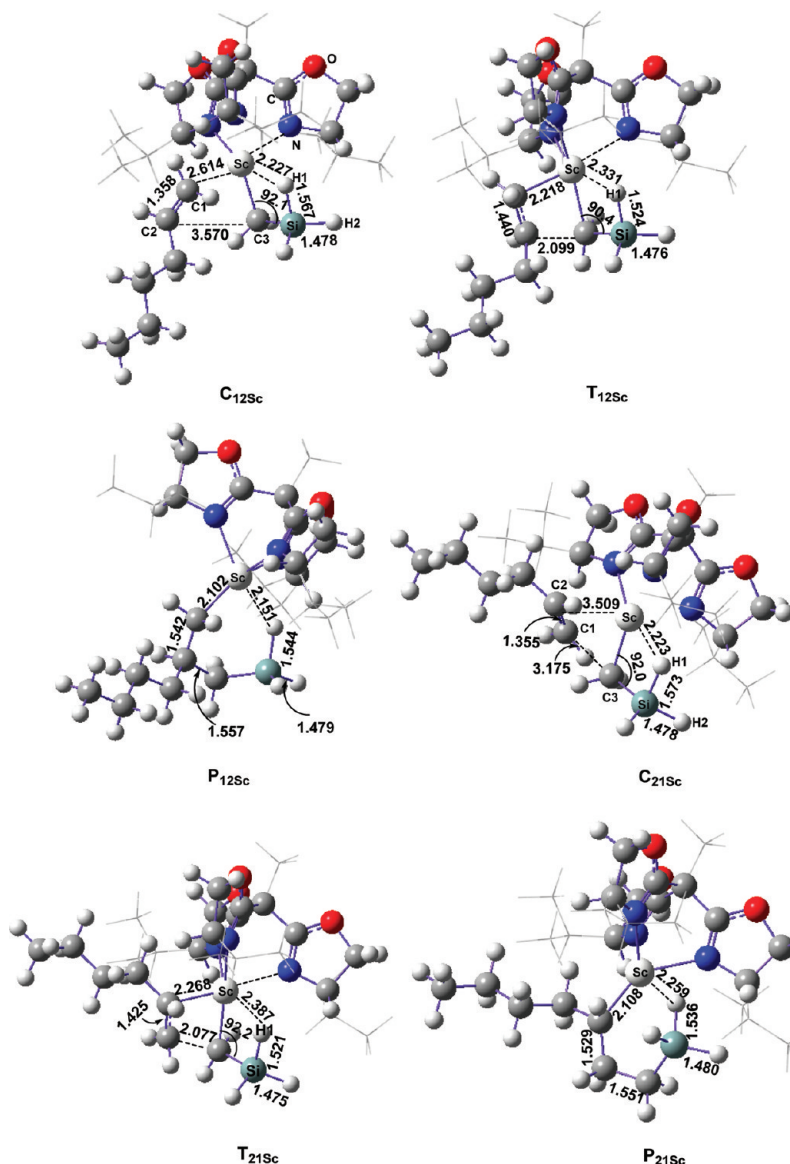


**Figure 3.** Geometric structures (distance in Å and angle in deg) involved in the energy profiles of 1,2- and 2,1-insertion of 1-hexene at the chain initiation stage.

Si···H1 and 90.4° for the Sc–CH<sub>2</sub>–Si angle) and that in T<sub>12Sc</sub> (2.387 Å for Sc–H1, 1.521 Å for Si–H1 and 92.2° for the Sc–CH<sub>2</sub>–Si angle) indicates the shorter Sc···H1 distance and smaller Sc–CH<sub>2</sub>–Si angle in T<sub>12Sc</sub>. This suggests that such an agostic interaction in T<sub>12Sc</sub> is stronger than that in T<sub>21Sc</sub> and may also account for the more stability of T<sub>12Sc</sub>. The similar geometrical feature was also observed when using the real structure of active species [Sc(iPr-trisox)(CH<sub>2</sub>SiMe<sub>3</sub>)]<sup>2+</sup> (see Figure S-5 in Supporting Information for more details).

To further access the regioselectivity in the chain propagation stage, the insertion of monomer into the Sc–CH<sub>2</sub> bond of P<sub>12Sc</sub> was also investigated. As the insertion of the first monomer does, both 1,2- and 2,1-insertions of the incoming monomer into the Sc–C bond of P<sub>12Sc</sub> were calculated, and the energy profiles are shown in Figure 4. As shown in this figure, the 1,2-insertion of the second monomer starts with the formation of complex C<sub>1212Iso</sub> (stereoselectivity discussed below, *vide infra*), which is slightly lower in free energy than the energy sum of separated P<sub>12Sc</sub> and m by 1.03 kcal/mol. This insertion

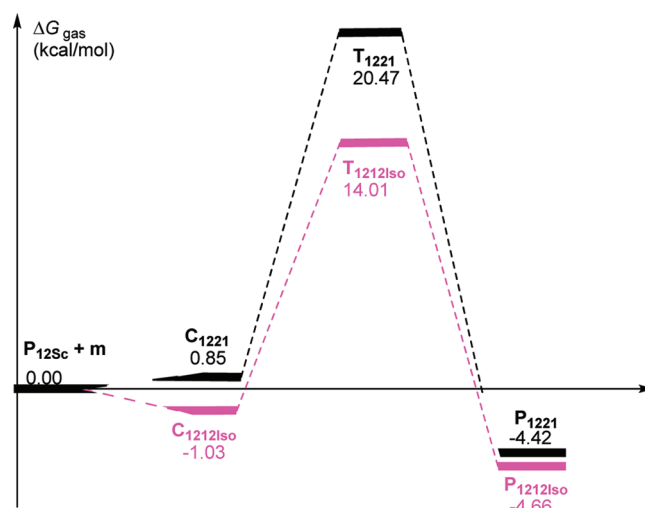


**Figure 4.** Computed energy profiles (energy in kcal/mol) for 1,2- and 2,1-insertion processes of 1-hexene at the chain propagation stage.

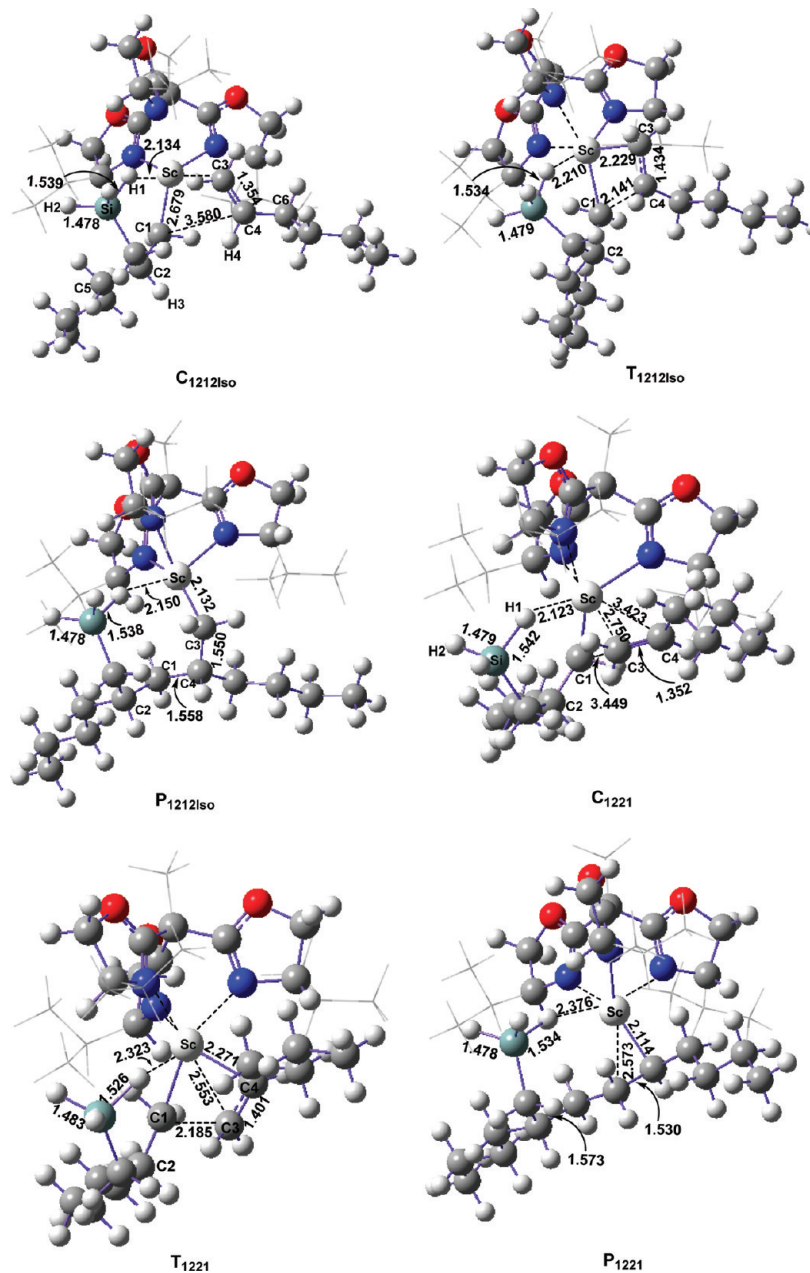


**Figure 5.** Geometric structures (distance in Å) involved in the energy profiles of 1,2- and 2,1-insertions of 1-hexene at the chain propagation stage.

process, which overcomes an energy barrier of 15.04 kcal/mol, is exergonic by 4.66 kcal/mol. Whereas, the 2,1-insertion process, which goes through prereaction complex C<sub>1221</sub> and transition state T<sub>1221</sub> leading to insertion product P<sub>1221</sub>, is kinetically less favorable in comparison with 1,2-insertion reaction. This is suggested by the higher insertion energy barrier of 20.47 kcal/mol for 2,1-insertion (15.04 kcal/mol for 1,2-insertion, Figure 4). However, the energetic superiority of 1,2-insertion manner is so slight since the relative free energies of for C<sub>1221</sub> (0.85 kcal/mol) and P<sub>1221</sub> (-4.42 kcal/mol) and are close to those for C<sub>1212Iso</sub> (-1.03 kcal/mol) and P<sub>1212Iso</sub> (-4.66 kcal/mol), respectively. To elucidate the origin of the kinetic preference of 1,2-insertion, we further analyzed the structures and energies of T<sub>1212Iso</sub> and T<sub>1221</sub>. As shown in Figure 5, the Sc–C3 distance of 2.229 Å and C1···C4 contact of 2.141 Å in T<sub>1212Iso</sub> are shorter than the corresponding interatomic distances in T<sub>1221</sub> (Sc–C4 distance of 2.271 and C1···C3 contact of 2.185 Å). This indicates that the

1-hexene moiety binds more tightly to the metal center of T<sub>1212Iso</sub> in comparison with that of T<sub>1221</sub>. A further analysis of energy decomposition of T<sub>1212Iso</sub> and T<sub>1221</sub> has also been carried out. The decomposition scheme is similar to that for T<sub>12Sc</sub> and T<sub>21Sc</sub> (*vide ante*). The interaction energies  $\Delta E_{\text{int}}$  between P<sub>12Sc</sub> and 1-hexene moieties in T<sub>1212Iso</sub> and in T<sub>1221</sub> are -35.16 and -24.98 kcal/mol, respectively, which could partly offset the unfavorable item  $\Delta E_{\text{def}}$  (total deformation energy, 42.04 kcal/mol for T<sub>1212Iso</sub> and 36.40 kcal/mol for T<sub>1221</sub>). Therefore, the  $\Delta E_{\text{TS}}$  (-35.16 + 42.04 = 6.88 kcal/mol) obtained for T<sub>1212Iso</sub> is lower than that (-24.98 + 36.40 = 11.42 kcal/mol) for T<sub>1221</sub>. Like the case of T<sub>12Sc</sub> and T<sub>21Sc</sub>, the less stability of T<sub>1221</sub> is mainly due to the weaker interaction between P<sub>12Sc</sub> and 1-hexene moiety. Furthermore, taking a closer look at the structures of T<sub>1212Iso</sub> and T<sub>1221</sub>, one may find that there are significant interactions between Sc and a H atom of SiH<sub>3</sub> in the preinserted CH<sub>2</sub>SiH<sub>3</sub> group, as suggested by the Sc···H distances (2.210 Å in T<sub>1212Iso</sub>

and 2.323 Å in  $T_{1221}$ ), the elongated Si–H bond lengths (1.534 Å in  $T_{1212\text{Iso}}$  and 1.526 Å in  $T_{1221}$ ) compared with the normal Si–H contact of 1.48 Å, and the more negative NBO charges (−0.33 in  $T_{1212\text{Iso}}$  and −0.31 in  $T_{1221}$ ) on the H atom interacting with Sc atom (Figure 5). In comparison with  $T_{1221}$ ,  $T_{1212\text{Iso}}$  has a shorter Sc···H distance (2.210 Å), longer Si–H bond length (1.534 Å), and more negative NBO charge (−0.33). As a whole, these geometrical and electronic features could account for the more stability of  $T_{1212\text{Iso}}$ .

## 2. Stereoselectivity in the 1-Hexene Polymerization.

To computationally interpret the stereoselectivity of 1-hexene polymerization observed experimentally, it is necessary to conduct calculations for both *iso*- and *syndio*-specific manners. The coordination of 1-hexene in 1,2-*si* and 1,2-*re* manner to the metal center of  $P_{12\text{Sc}}$  could lead to the *iso*- and *syndio*-tactic polymers, respectively. Figure 6 shows the computed energy

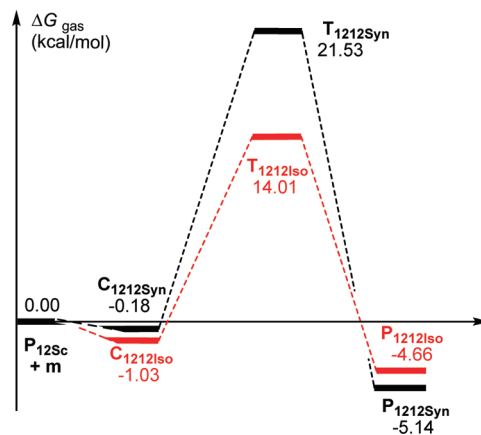


**Figure 6.** Computed energy profiles (energy in kcal/mol) for isotactic and syndiotactic insertion processes of 1-hexene.

profile for *re*-coordination of 1-hexene to the metal center of  $P_{12\text{Sc}}$  and subsequent insertion process. Since  $C_{1212\text{Iso}}$  shows the *si*-coordination fashion of 1-hexene (Figure 5) and the resulting product  $P_{1212\text{Iso}}$  is isospecific, the energy profile for the process of  $C_{1212\text{Iso}} \rightarrow T_{1212\text{Iso}} \rightarrow P_{1212\text{Iso}}$  (Figure 4) is also included in Figure 6 for comparison. As shown in this figure, the isospecific insertion of 1-hexene starts with its *si*-coordination to metal center (formation of  $C_{1212\text{Iso}}$ ), and goes through a transition state  $T_{1212\text{Iso}}$  leading to corresponding product  $P_{1212\text{Iso}}$ . However, the syndiospecific insertion occurs through the *re*-coordination of monomer to the metal center and then proceeds via a transition state  $T_{1212\text{Syn}}$  to give insertion product  $P_{1212\text{Syn}}$ . In comparison, the lower insertion free-energy barrier of 15.04 kcal/mol for  $T_{1212\text{Iso}}$  lends kinetic advantage to isotactic polymerization over syndiotactic polymerization, which has a higher insertion energy barrier of 21.71 kcal/mol (Figure 6). The syndiospecific product and the isospecific enantiomer are almost isoenergetic (energy difference of 0.48 kcal/mol, Figure 6). That is to say, the microstructure of polymer is mainly controlled by kinetics. In this sense, the current computational results are in agreement with the isoselectivity observed experimentally.

For better understanding of the origin of isospecific polymerization, the structure characters of some stationary points have been analyzed. In  $C_{1212\text{Iso}}$ , the 1-hexene moiety interacts with the metal center via *si*-coordination, which gives rise to isospecific product  $P_{1212\text{Iso}}$  with *R*-configuration (refer to the chiral C4 atom, see Figure 5). Such a *si*-coordination manner

could avoid the repulsive interaction between the polymer chain and the  $(\text{CH}_2)_3\text{CH}_3$  group of the coordinated 1-hexene moiety (see  $C_{1212\text{Iso}}$  and  $T_{1212\text{Iso}}$  in Figure 5). While, the *re*-coordination of the incoming monomer resulted in significant repulsion between the polymer chain and the  $(\text{CH}_2)_3\text{CH}_3$  group of the coordinated 1-hexene moiety (see  $C_{1212\text{Syn}}$  and  $T_{1212\text{Syn}}$  in Figure 7). Such repulsion could destabilize  $T_{1212\text{Syn}}$ .

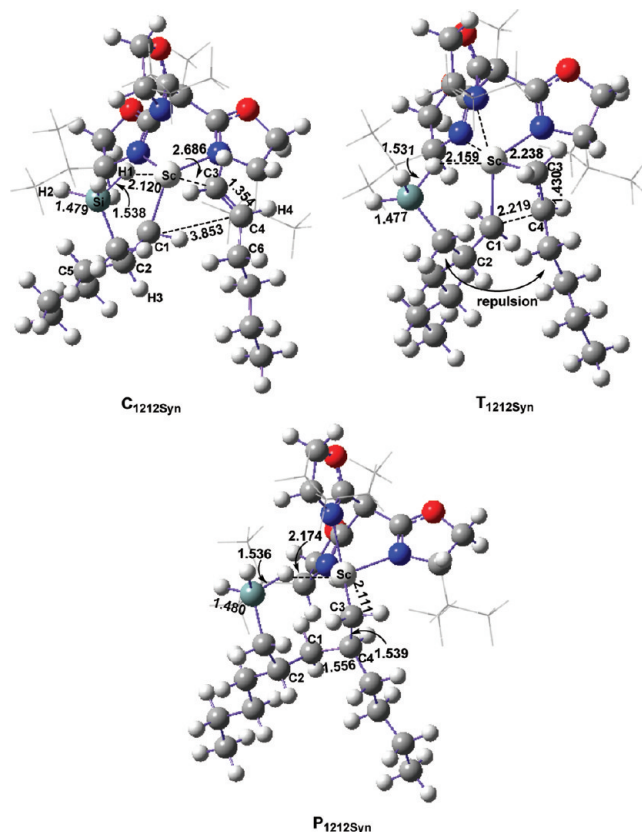


**Figure 7.** Geometric structures (distance in Å) involved in the energy profile of the syndiotactic insertion process.

The *re*-coordination manner could lead to syndiotactic product  $P_{1212\text{Syn}}$  with *S*-configuration (refer to the chiral C4 atom). It is therefore concluded that the steric effects of the growing chain-end could be the main factor governing the stereoselectivity in this system.

**3. Activity Comparison of Dicationic and Monocationic Species.** Experimental studies have shown that the dicationic species  $[\text{Sc}(\text{iPr-trisox})(\text{CH}_2\text{SiMe}_3)]^{2+}$  has higher activity for 1-hexene polymerization than the monocationic analogue  $[\text{Sc}(\text{iPr-trisox})(\text{CH}_2\text{SiMe}_3)_2]^+$  by 3 orders of magnitude.<sup>7a</sup> For comparison, calculations on  $[\text{Sc}(\text{iPr-trisox})(\text{CH}_2\text{SiH}_3)_2]^+ (2_{\text{Sc}}')$  modeling the monocation of  $2_{\text{Sc}}$  has been also performed. The computed energy profile is shown in Figure 8. The energy profile for  $3_{\text{Sc}}'$ -involved process  $C_{12\text{Sc}} \rightarrow T_{12\text{Sc}} \rightarrow P_{12\text{Sc}}$  is also included in this figure for convenience in discussion. Insertion processes catalyzed by monocationic  $2_{\text{Sc}}'$  and dicationic  $3_{\text{Sc}}'$  start with the formations of prereaction complexes  $C_{\text{MC}}$  and  $C_{12\text{Sc}}$  and then goes through four-center transition states  $T_{\text{MC}}$  and  $T_{12\text{Sc}}$  to give the insertion products  $P_{\text{MC}}$  and  $P_{12\text{Sc}}$ , respectively. The coordination complex  $C_{12}$  (complexation energy of −2.37 kcal/mol) is more stable than  $C_{\text{MC}}$  (complexation energy of 7.42 kcal/mol). The complex  $C_{\text{MC}}$  is higher in free energy by 7.42 kcal/mol in comparison

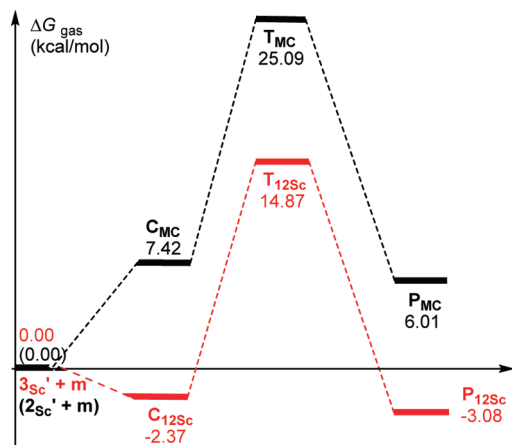


**Figure 8.** Computed energy profiles (energy in kcal/mol) for 1-hexene polymerization catalyzed by dication ( $3_{\text{Sc}}'$ ) and monocation ( $2_{\text{Sc}}'$ ) species at the chain initiation stage.

with separated species ( $2_{\text{Sc}}' + \text{m}$ ). The higher relative free energy of 7.42 kcal/mol for  $\text{C}_{\text{MC}}$  could be due to overestimation of translational entropy in gas-phase. The insertion process catalyzed by  $3_{\text{Sc}}'$  has a lower free-energy barrier of 17.24 kcal/mol and is exergonic by -3.08 kcal/mol. This process is both kinetically and energetically favorable than the  $2_{\text{Sc}}'$ -catalyzed one (free-energy barrier of 25.09 kcal/mol and endergonic by 6.01 kcal/mol). In the  $2_{\text{Sc}}'$ -catalyzed process, the

endergonic feature and the insertion energy barrier of 25.09 kcal/mol, which is higher than that (~20 kcal/mol) for the usual olefin insertion reaction, could add better understanding to the fact that the monocationic species has a very low activity toward 1-hexene polymerization.<sup>7a</sup>

Geometrically, the two alkyl groups of  $2_{\text{Sc}}'$  (Figure 9) make their respective metal centers more crowded in comparison with  $3_{\text{Sc}}'$  (Figure 1) having one alkyl group. Such a situation sterically hampered the binding of 1-hexene moiety to the metal center of  $2_{\text{Sc}}'$ , which accounts for the less stabilities of  $\text{C}_{\text{MC}}$  and  $\text{T}_{\text{MC}}$  in comparison with  $\text{C}_{12\text{Sc}}$  and  $\text{T}_{12\text{Sc}}$ , respectively. To further access the origin of the higher activity of  $3_{\text{Sc}}'$ , the analyses of energy and electronic character have also been performed. The interaction energy  $\Delta E_{\text{int}}$  between 1-hexene moiety and the active species ( $i\text{Pr}-\text{trisox})\text{Sc}(\text{CH}_2\text{SiH}_3)_2^{+}$  in  $\text{T}_{12\text{Sc}}$  and ( $i\text{Pr}-\text{trisox})\text{Sc}(\text{CH}_2\text{SiH}_3)_2^{+}$  in  $\text{T}_{\text{MC}}$  were computed to be -37.21 and -23.37 kcal/mol, respectively. The sum of deformation energy  $\Delta E_{\text{def}}$  of the active species and the 1-hexene moiety were computed to be 43.93 and 38.28 kcal/mol for  $\text{T}_{12\text{Sc}}$  and in  $\text{T}_{\text{MC}}$ , respectively. The energy of TS ( $\Delta E_{\text{TS}}$ ) could be obtained for  $\text{T}_{12\text{Sc}}$  ( $-37.21 + 43.93 = 6.72$  kcal/mol) and  $\text{T}_{\text{MC}}$  ( $-23.37 + 38.28 = 14.91$  kcal/mol), respectively. Therefore, the less stability of  $\text{T}_{\text{MC}}$  could be due to the weaker interaction between the ( $i\text{Pr}-\text{trisox})\text{Sc}(\text{CH}_2\text{SiH}_3)_2^{+}$  species and the 1-hexene moiety in  $\text{T}_{\text{MC}}$ . To get more insights on the different activities of the monocationic and dicationic species, the frontier orbital energies of the related cations were also analyzed on the basis of their optimized geometries. The dication

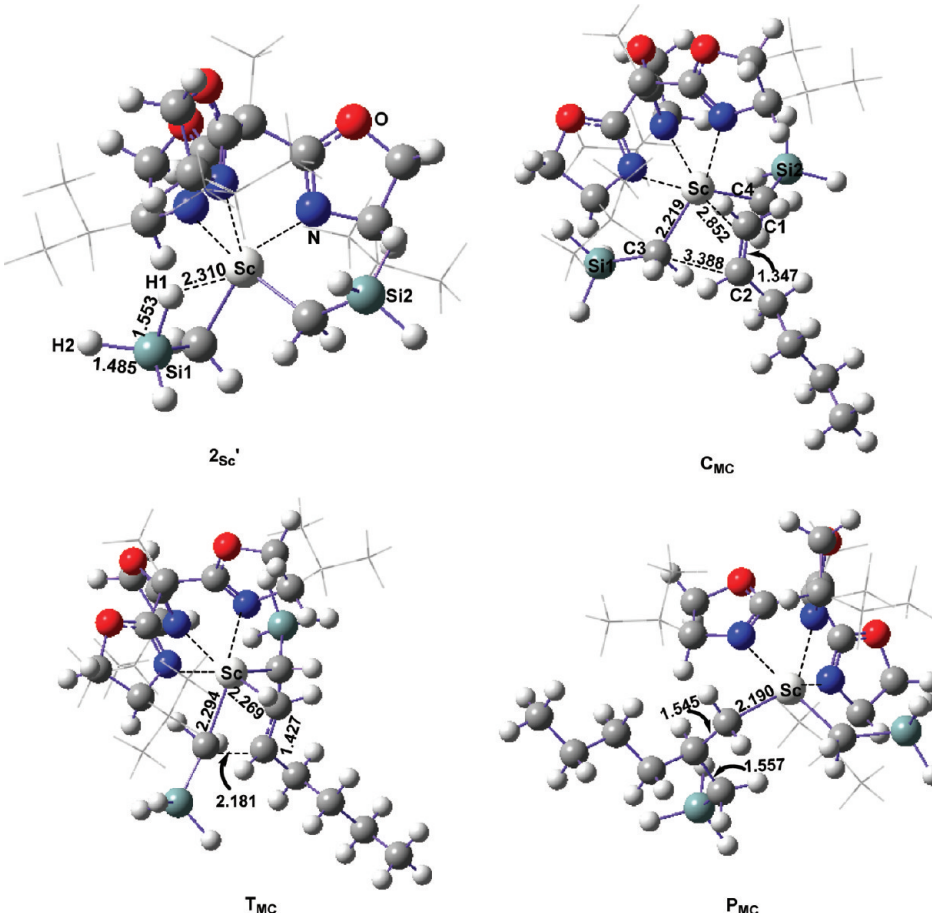


**Figure 9.** Geometric structures (distance in Å) involved in the energy profiles of 1-hexene polymerization catalyzed by monocation  $2_{\text{Sc}}'$  species at the chain initiation stage.

of  $3_{\text{Sc}}$  is more electron-deficient and is a stronger Lewis acid with bigger chemical hardness (computed to be 2.847 eV, derived from the energies of frontier orbitals) compared to monocation of  $2_{\text{Sc}}$  (chemical hardness of 2.603 eV), which could account for the higher reactivity of dication toward electron-rich olefin. Our calculations also show that the LUMO energies of the cations of  $3_{\text{Sc}}$  and  $2_{\text{Sc}}$  are  $-0.3112 \text{ au}$  and  $-0.1718 \text{ au}$ , respectively, and the HOMO energy of 1-hexene is  $-0.2591 \text{ au}$ . By comparison, the HOMO energy of 1-hexene is closer to the LUMO energy of the dication, suggesting that 1-hexene is easier to react with the dication in comparison with the monocationic analogue.

**4. Activity Comparison of (*i*Pr-trisox)Sc( $\text{CH}_2\text{SiMe}_3$ ) $^{2+}$  with (*i*Pr-trisox)Y( $\text{CH}_2\text{SiMe}_3$ ) $^{2+}$  Species.** It was experimentally found that the Sc active species possesses significantly higher catalytic activity toward 1-hexene polymerization compared with the Y analogue. This motivated us to computationally elucidate the origin of the difference in activity. The computed energy profile for the reaction of 1-hexene with  $3_Y'$  (the Y analogue of  $3_{\text{Sc}}$ ) and the related structures are shown in Figure 10 and 11, respectively. For a comparison, the

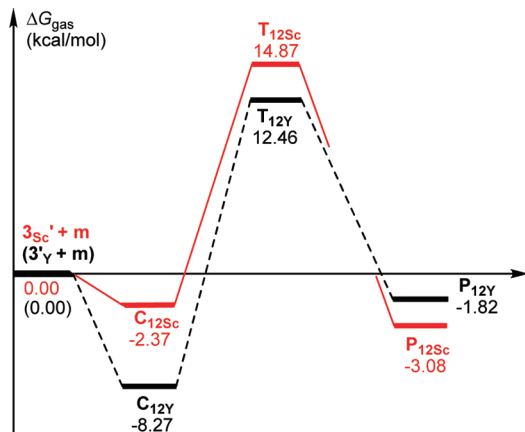


**Figure 10.** Computed energy profiles (energy in kcal/mol) for 1-hexene polymerization catalyzed by  $3_{\text{Sc}}'$  and  $3'_Y$  species at the chain initiation stage.

corresponding energy profile for  $3_{\text{Sc}}'$ -containing system is also included in this figure. Like  $3_{\text{Sc}}'$ , the structure of  $3'_Y$  (Figure 11) also shows a  $\beta$ -Si–H agostic interaction as suggested by the Y–H1 distance of 2.309 Å, the Si–H1 bond length of 1.590 Å, and the Y–C3–Si angle of 92.8°. As shown in Figure 10, the complexation energy of  $C_{12\text{Y}}$  ( $-8.27 \text{ kcal/mol}$ ) is lower than that of  $C_{12\text{Sc}}$  ( $-2.37 \text{ kcal/mol}$ ). The insertion energy barrier of 20.73 kcal/mol for  $3'_Y$  assisted insertion reaction is larger than that (17.24 kcal/mol) for  $3_{\text{Sc}}'$ -involved reaction. The insertion product  $P_{12\text{Y}}$  is also slightly less stable than  $P_{12\text{Sc}}$  by 1.26 kcal/mol. However, the relative energy (12.46 kcal/mol) of  $3'_Y$ -involved insertion transition state ( $T_{12\text{Y}}$ ) is slightly lower than that (14.87 kcal/mol) of  $T_{12\text{Sc}}$ . The energy profile shown in Figure 10 indicates that the larger insertion barrier for  $3'_Y$  reaction system is mainly due to the lower  $C_{12\text{Y}}$  in energy in comparison with  $3_{\text{Sc}}'$ -containing system. The chemical hardness of (*i*Pr-trisox)Sc( $\text{CH}_2\text{SiMe}_3$ ) $^{2+}$  and (*i*Pr-trisox)Y( $\text{CH}_2\text{SiMe}_3$ ) $^{2+}$  were computed to be 2.847 and 2.751 eV, respectively, suggesting a stronger Lewis acidity and hence higher reactivity of the former toward olefin in comparison with the later.

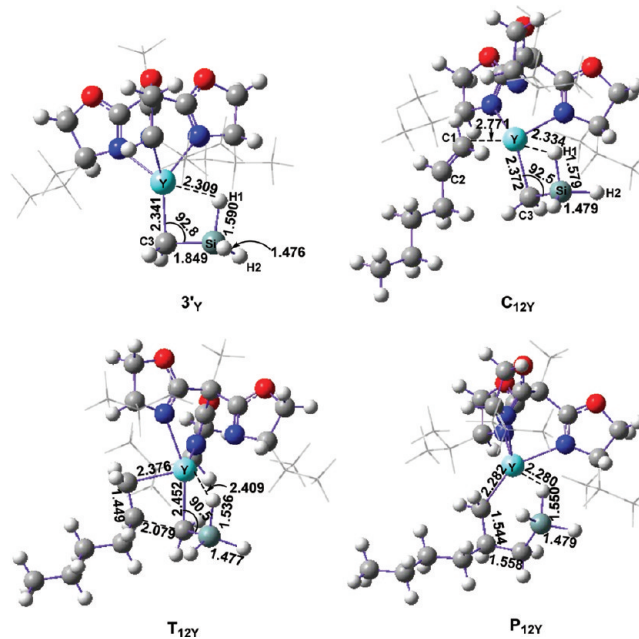


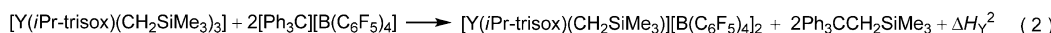
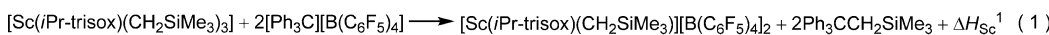
**Figure 11.** Geometric structures (distance in Å and angle in degree) involved in the energy profiles of 1-hexene polymerization catalyzed by  $3_{\text{Sc}}'$  and  $3'_Y$  species at the chain initiation stage.

To cast a light on the reason for the stability of  $C_{12\text{Y}}$ , energy decomposition analyses of  $C_{12\text{Sc}}$  and  $C_{12\text{Y}}$  (electronic energy,  $\Delta E$ ) were carried out in a similar manner described above. The complex  $C_{12\text{Sc}}$  (or  $C_{12\text{Y}}$ ) can be divided into two fragments, viz.  $3_{\text{Sc}}'$  (or  $3'_Y$ ) species and 1-hexene moiety. The following information was obtained for  $C_{12\text{Sc}}$ :  $\Delta E_{\text{int}} = -23.22 \text{ kcal/mol}$ ,  $\Delta E_{\text{def}}(3_{\text{Sc}}') = 8.79 \text{ kcal/mol}$ ,  $\Delta E_{\text{def}}(1\text{-hexene}) = 2.51 \text{ kcal/mol}$ ; and therefore  $\Delta E(C_{12\text{Sc}}) = -23.22 + 8.79 + 2.51 = -11.92 \text{ kcal/mol}$ . While the following components were obtained for  $C_{12\text{Y}}$ :  $\Delta E_{\text{int}} = -25.10 \text{ kcal/mol}$ ;  $\Delta E_{\text{def}}(3'_Y) = 5.65 \text{ kcal/mol}$ ;  $\Delta E_{\text{def}}(1\text{-hexene}) = 2.51 \text{ kcal/mol}$ ; and therefore  $\Delta E(C_{12\text{Y}}) = -25.10 + 5.65 + 2.51 = -16.94 \text{ kcal/mol}$ , which is lower than that ( $-11.92 \text{ kcal/mol}$ ) of  $C_{12\text{Sc}}$ . It is obvious that the lower  $\Delta E_{\text{int}}$  for  $C_{12\text{Y}}$  and less deformation energy of  $\Delta E_{\text{def}}(3'_Y)$  account for the more stability of  $C_{12\text{Y}}$  in comparison with  $C_{12\text{Sc}}$ .

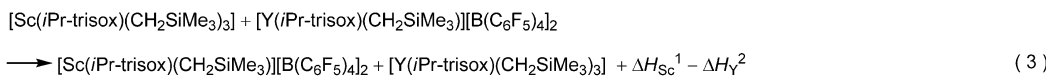
Although the  $3'_Y$  assisted insertion of 1-hexene is less favorable both kinetically and energetically than the  $3_{\text{Sc}}'$  involved process, such low superiorities are hard to explain well the large difference in activity between the Sc active species and its Y analogue. This drove us to further access the formations of the two kinds of active species and their interactions with counterion, respectively.

According to experimental findings,<sup>7a</sup> the reaction of the trialkyl precursor  $[(i\text{Pr-trisox})\text{Ln}(\text{CH}_2\text{SiMe}_3)_3]$  ( $\text{Ln} = \text{Sc}, \text{Y}$ ) with 2 equiv of the borate compound  $[\text{Ph}_3\text{C}] [\text{B}(\text{C}_6\text{F}_5)_4]$  gives rise to 1 equiv of the contact ion-pair  $[\text{Ln}(i\text{Pr-trisox})(\text{CH}_2\text{SiMe}_3)]^- [\text{B}(\text{C}_6\text{F}_5)_4]_2$  and 2 equiv of  $\text{Ph}_3\text{CCH}_2\text{SiMe}_3$ , as illustrated by reactions 1 and 2 in Scheme 3. The optimized structures of the contact ion-pairs are shown in Figure 12. As shown in this figure, the counterions coordinate to the metal atom Sc (or Y) via three F atoms, viz. F1 and F2 atom in one counterion and F3 atom in another one (Figure 12). We assume that the reaction enthalpies of reactions 1 and 2 are  $\Delta H_{\text{Sc}}^1$  and  $\Delta H_{\text{Y}}^2$  (Scheme 3), respectively. Let (1) minus (2) give (3), and the reaction enthalpy of (3) is therefore  $\Delta H_{\text{Sc}}^1 - \Delta H_{\text{Y}}^2$ . Let  $\Delta H = \Delta H_{\text{Sc}}^1 - \Delta H_{\text{Y}}^2$ . According to the calculated enthalpies based on optimized structures of  $[(i\text{Pr-trisox})\text{Ln}(\text{CH}_2\text{SiMe}_3)_3]$  and

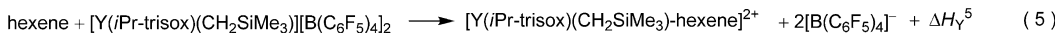
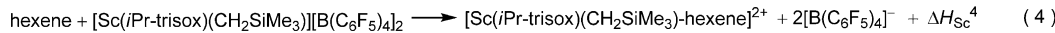
**Scheme 3. Formation Process of Active Species  $[\text{Ln}(\text{iPr-trisox})(\text{CH}_2\text{SiMe}_3)][\text{B}(\text{C}_6\text{F}_5)_4]_2$  ( $\text{Ln} = \text{Sc}$  and  $\text{Y}$ ) and the Separation of Ion Pairs via Hexene Coordination**



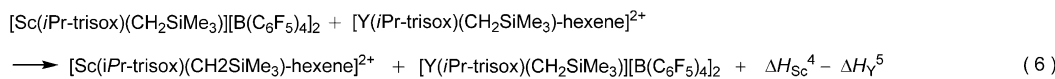
(1) – (2) :



$$\Delta H^3 = \Delta H_{\text{Sc}}^1 - \Delta H_{\text{Y}}^2 = -5.96 \text{ kcal/mol}$$



(4) – (5) :



$$\Delta H^6 = \Delta H_{\text{Sc}}^4 - \Delta H_{\text{Y}}^5 = -6.00 \text{ kcal/mol}$$

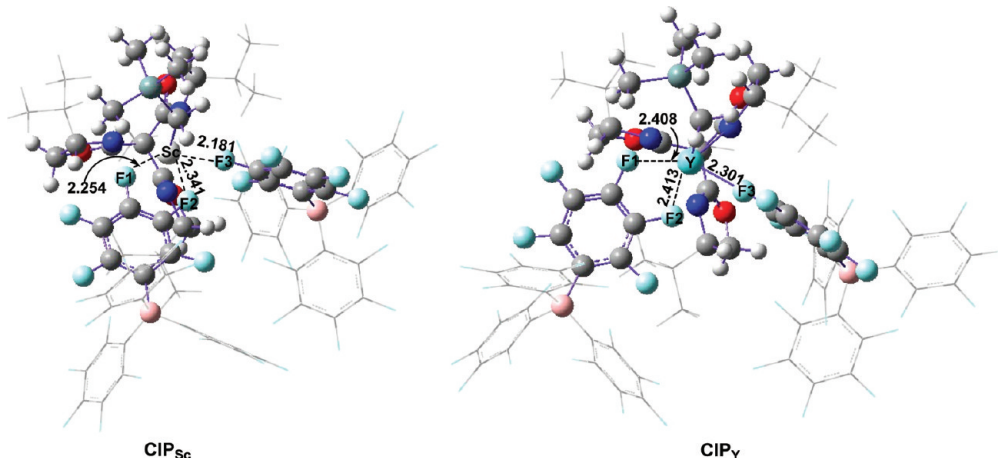


**Figure 12.** Optimized structures for contact ion-pair  $[\text{Ln}(\text{iPr-trisox})(\text{CH}_2\text{SiMe}_3)][\text{B}(\text{C}_6\text{F}_5)_4]_2$  ( $\text{CIP}_{\text{Sc}}$ ,  $\text{Ln} = \text{Sc}$ ;  $\text{CIP}_{\text{Y}}$ ,  $\text{Ln} = \text{Y}$ ).

$[\text{Ln}(\text{iPr-trisox})(\text{CH}_2\text{SiMe}_3)][\text{B}(\text{C}_6\text{F}_5)_4]_2$ , ( $\text{Ln} = \text{Sc}, \text{Y}$ ) shown in eq 3, the reaction enthalpy of (3), viz.  $\Delta H^3 = \Delta H_{\text{Sc}}^1 - \Delta H_{\text{Y}}^2$ , was computed to be  $-5.96 \text{ kcal/mol}$ . The negative value of  $\Delta H^3$  suggests that eq 1 is more exothermic (or less endothermic) than eq 2. That is to say, it is thermodynamically easier for Sc trialkyl precursor to be activated by  $[\text{Ph}_3\text{C}][\text{B}(\text{C}_6\text{F}_5)_4]$  and to give corresponding active species in comparison with the Y trialkyl complex. This could account for the higher activity of Sc species compared with Y analogue. Similarly, the difference in the enthalpies required for the reactions of hexene with the contacted ion pairs ( $\text{CIP}_{\text{Sc}}$  or  $\text{CIP}_{\text{Y}}$  in Figure 12) leading to the anion and hexene-complexed cation, as shown in eqs 4 and 5 in Scheme 3, could be also computed. We assume that the reaction enthalpies of (4) and (5) are  $\Delta H_{\text{Sc}}^4$  and  $\Delta H_{\text{Y}}^5$  (Scheme 3), respectively. Let (4) minus (5) give (6), and the reaction enthalpy of (6) is therefore  $\Delta H_{\text{Sc}}^4 - \Delta H_{\text{Y}}^5$ . Let  $\Delta H^6 = \Delta H_{\text{Sc}}^4 - \Delta H_{\text{Y}}^5$ . In eqs 4–6, the  $[\text{Sc}(\text{iPr-trisox})(\text{CH}_2\text{SiMe}_3)\text{-hexene}]^{2+}$  is actually the  $\text{C}_{12\text{Sc}}$  shown in Figure 3, and the  $[\text{Y}(\text{iPr-trisox})(\text{CH}_2\text{SiMe}_3)\text{-hexene}]^{2+}$  is actually the  $\text{C}_{12\text{Y}}$  shown in Figure 11. Like eq 3,

according to the calculated enthalpies of optimized structures, the reaction enthalpy of (6), viz.  $\Delta H^6 = \Delta H_{\text{Sc}}^4 - \Delta H_{\text{Y}}^5$ , was computed to be  $-6.00 \text{ kcal/mol}$ . The negative value of  $\Delta H^6$  illustrates that the two anions of ion pair  $\text{CIP}_{\text{Sc}}$  is easier to be replaced by hexene to coordinate to the metal center in comparison with that of ion pair  $\text{CIP}_{\text{Y}}$ . This result could also account for the higher activity of Sc system in comparison with Y analogue.

## CONCLUSION

We have computationally studied the regio- and stereoselectivity of the polymerization of 1-hexene catalyzed by the dicationic rare-earth metal complexes  $[(\text{iPr-trisox})\text{Ln}(\text{CH}_2\text{SiMe}_3)]^{2+}$  ( $\text{Ln} = \text{Sc}$  and  $\text{Y}$ ). At both chain initiation and propagation stages, 1,2-insertion has been found to be kinetically favorable over 2,1-insertion. The kinetic priority of 1,2-insertion pattern is mainly due to the absence of repulsive interaction between the ancillary ligand and the  $\text{CH}_3(\text{CH}_2)_3$  group of 1-hexene moiety in the insertion transition state and the resulting stronger binding between the metal center and the

1-hexene motif. The stereoselectivity has been found to follow chain-end mechanism, and the iso-specific insertion of 1-hexene observed experimentally is mainly controlled by kinetics. The insertion reaction catalyzed by dicationic active species is easier than that by monocationic species both kinetically and energetically, which is in agreement with the higher activity of the dicationic species observed experimentally. The features of frontier molecular orbitals of the two kinds of species could also account for their different activities. The origin of difference in activity between the scandium active species and its yttrium analogue has been also computationally investigated. It has been found that the scandium-catalyzed insertion reaction has kinetic preference over the yttrium-catalyzed reaction and that the generation of scandium active species is easier compared with that of yttrium analogue. These results could help understand better the higher activity of the scandium complex than its yttrium analogue and develop rare earth polymerization catalysts.

## ■ ASSOCIATED CONTENT

### Supporting Information

Figures giving the energy profiles of 1,2- and 2,1-insertion process computed at the levels of B3LYP and MPW1K, optimized structures with  $\text{CH}_2\text{SiMe}_3$  group, and tables giving the optimized Cartesian coordinates, total energies, and the imaginary frequencies of TSs. This material is available free of charge via the Internet at <http://pubs.acs.org>.

## ■ AUTHOR INFORMATION

### Corresponding Author

\*E-mail: luoyi@dlut.edu.cn (Y.L.); houz@riken.jp (Z.H.); qujp@dlut.edu.cn (J.Q.).

## ■ ACKNOWLEDGMENTS

This work was partly supported by the National Natural Science Foundation of China (No. 21028001, 21174023, 21137001, 20806012). Y.L. thanks the SEM Scientific Research Funding for ROCS. Z.H. acknowledges financial support from China's Thousand Talents Program. The authors also thank RICC (RIKEN Integrated Cluster of Clusters) and the Network and Information Center of Dalian University of Technology for computational resources.

## ■ REFERENCES

- (1) Recent reviews: (a) Gibson, V. C.; Spitzmesser, S. K. *Chem. Rev.* **2003**, *103*, 283–315. (b) Bochmann, M. *J. Organomet. Chem.* **2004**, *689*, 3982–3998. (c) Park, S.; Han, Y.; Kim, S. K.; Lee, J.; Kim, H. K.; Do, Y. *J. Organomet. Chem.* **2004**, *689*, 4263–4276. (d) Bolton, P. D.; Mountford, P. *Adv. Synth. Catal.* **2005**, *347*, 355–366. (e) Domski, G. J.; Rose, J. M.; Coates, G. W.; Bolig, A. D.; Brookhart, M. *Prog. Polym. Sci.* **2007**, *32*, 30–92. (f) Takeuchi, D. *Dalton Trans.* **2010**, *39*, 311–328.
- (2) (a) Babu, G. N.; Newmark, R. A. *Macromolecules* **1994**, *27*, 3383–3388. (b) Yamaguchi, Y.; Suzuki, N.; Mise, T.; Wakatsuki, Y. *Organometallics* **1999**, *18*, 996–1001. (c) Tshuva, E. Y.; Goldberg, I.; Kol, M. *J. Am. Chem. Soc.* **2000**, *122*, 10706–10707. (d) Groysman, S.; Goldberg, I.; Kol, M.; Genizi, E.; Goldschmidz, Z. *Inorg. Chim. Acta* **2003**, *345*, 137–144. (e) Segal, S.; Goldberg, I.; Kol, M. *Organometallics* **2005**, *24*, 200–202. (f) Vijayakrishna, K.; Sundararajan, G. *Polymer* **2006**, *47*, 3363–3371. (g) Sudhakar, P.; Sundararajan, G. *J. Polym. Sci., Part A: Polym. Chem.* **2006**, *44*, 4006–4014. (h) Sudhakar, P. *J. Polym. Sci., Part A: Polym. Chem.* **2007**, *45*, 5470–5479. (i) Domski, G. J.; Lobkovsky, E. B.; Coates, G. W. *Macromolecules* **2007**, *40*, 3510–3513. (j) Ishii, A.; Toda, T.; Nakata, N.; Matsuo, T. *J. Am. Chem. Soc.* **2009**, *131*, 13566–13567. (k) Cohen, A.; Kopilov, J.; Lamberti, M.; Venditto, V.; Kol, M. *Macromolecules* **2010**, *43*, 1689–1691.
- (3) Selected reviews: (a) Nishiura, M.; Hou, Z. *Nat. Chem.* **2010**, *2*, 257–268. (b) Rodrigues, A. S.; Carpentier, J. F. *Coord. Chem. Rev.* **2008**, *252*, 2137–2154. (c) Li, X.; Hou, Z. *Coord. Chem. Rev.* **2008**, *252*, 1842–1869. (d) Zeimentz, P. M.; Arndt, S.; Elvidge, B. R.; Okuda, J. *Chem. Rev.* **2006**, *106*, 2404–2433. (e) Kretschmer, W. P.; Meetsma, A.; Hessen, B.; Schmalz, T.; Sadaf, Q.; Kempe, R. *Chem. A. Eur. J.* **2006**, *12*, 8969–8978. (f) Hou, Z.; Wakatsuki, Y. *Coord. Chem. Rev.* **2002**, *231*, 1–22. (g) Evans, W. J.; Davis, B. L. *Chem. Rev.* **2002**, *102*, 2119–2136. (h) Marques, M.; Sella, A.; Takats, J. *Chem. Rev.* **2002**, *102*, 2137–2160. (i) Chen, E. Y. X.; Marks, T. J. *Chem. Rev.* **2000**, *100*, 1391–1434.
- (4) (a) Luo, Y.; Baldamus, J.; Hou, Z. *J. Am. Chem. Soc.* **2004**, *126*, 13910–13911. (b) Zhang, L.; Luo, Y.; Hou, Z. *J. Am. Chem. Soc.* **2005**, *127*, 14562–14563. (c) Li, X.; Hou, Z. *Macromolecules* **2005**, *38*, 6767–6769. (d) Li, X. F.; Baldamus, J.; Nishiura, M.; Tardif, O.; Hou, Z. *M. Angew. Chem., Int. Ed.* **2006**, *45*, 8184–8188. (e) Li, X. F.; Nishiura, M.; Mori, K.; Mashiko, T.; Hou, Z. *M. Chem. Commun.* **2007**, *4137*–4139. (f) Yu, N.; Nishiura, M.; Li, X. F.; Xi, Z. F.; Hou, Z. *M. Chem. Asian J.* **2008**, *3*, 1406–1414. (g) Zhang, H.; Luo, Y.; Hou, Z. *Macromolecules* **2008**, *41*, 1064–1066. (h) Li, X.; Nishiura, M.; Hu, L.; Mori, K.; Hou, Z. *J. Am. Chem. Soc.* **2009**, *131*, 13870–13882. (i) Li, X.; Hou, Z. *Macromolecules* **2010**, *43*, 8904–8909. (j) Pan, L.; Zhang, K.; Nishiura, M.; Hou, Z. *Macromolecules* **2010**, *43*, 9591–9593. (k) Guo, F.; Nishiura, M.; Koshino, H.; Hou, Z. *Macromolecules* **2011**, *44*, 6335–6344. (l) Guo, F.; Nishiura, M.; Koshino, H.; Hou, Z. *Macromolecules* **2011**, *44*, 2400–2403. (m) Pan, L.; Zhang, K.; Nishiura, M.; Hou, Z. *Angew. Chem., Int. Ed.* **2011**, DOI: 10.1002/anie.201104011.
- (5) (a) Luo, Y. J.; Hou, Z. *Stud. Surf. Sci. Catal.* **2006**, *161*, 95–104. (b) Hou, Z.; Luo, Y. J.; Li, X. *J. Organomet. Chem.* **2006**, *691*, 3114–3121.
- (6) Tredget, C. S.; Bonnet, F.; Cowley, A. R.; Mountford, P. *Chem. Commun.* **2005**, *3301*–3303.
- (7) (a) Ward, B. D.; Bellemín-Lapponaz, S.; Gade, L. H. *Angew. Chem., Int. Ed.* **2005**, *44*, 1668–1671. (b) Lukešová, L.; Ward, B. D.; Bellemín-Lapponaz, S.; Wadeohl, H.; Gade, L. H. *Dalton Trans.* **2007**, 920–922. (c) Lukešová, L.; Ward, B. D.; Bellemín-Lapponaz, S.; Wadeohl, H.; Gade, L. H. *Organometallics* **2007**, *26*, 4652–4657. (d) Ward, B. D.; Lukešová, L.; Wadeohl, H.; Bellemín-Lapponaz, S.; Gade, L. H. *Eur. J. Inorg. Chem.* **2009**, 866–871.
- (8) Reviews, see: (a) Rappe, A. K.; Skiff, W. M.; Casewit, C. J. *Chem. Rev.* **2000**, *100*, 1435–1456. (b) Niu, S.; Hall, M. B. *Chem. Rev.* **2000**, *100*, 353–406. (c) Michalak, A.; Ziegler, T. In *Computational Modeling of Homogeneous Catalysis*; Feliu, M., Agusti, L., Eds., Kluwer: Dordrecht, The Netherlands, 2002; Vol. 25, pp 57–78. (d) Tobisch, S. *Acc. Chem. Res.* **2002**, *35*, 96–104. (e) Bo, C.; Maseras, F. *Dalton Trans.* **2008**, 2911–2919. (f) Mandal, S. K.; Roesky, H. W. *Acc. Chem. Res.* **2010**, *43*, 248–259.
- (9) Examples, see: (a) Woo, T. K.; Ziegler, T. *Organometallics* **1994**, *13*, 2252–2261. (b) Xu, Z.; Vanka, K.; Firman, T.; Michalak, A.; Zurek, E.; Zhu, C.; Ziegler, T. *Organometallics* **2002**, *21*, 2444–2453. (c) Flisak, Z.; Ziegler, T. *Macromolecules* **2005**, *38*, 9865–9872. (d) Margl, P.; Deng, L.; Ziegler, T. *J. Am. Chem. Soc.* **1998**, *120*, 5517–5525. (e) Froese, R. D. J.; Musaev, D. G.; Morokuma, K. *Organometallics* **1999**, *18*, 373–379. (f) Froese, R. D. J.; Musaev, D. G.; Matsubara, T.; Morokuma, K. *J. Am. Chem. Soc.* **1997**, *119*, 7190–7196. (g) Musaev, D. G.; Froese, R. D. J.; Svensson, M.; Morokuma, K. *J. Am. Chem. Soc.* **1997**, *119*, 367–374. (h) Froese, R. D. J.; Musaev, D. G.; Morokuma, K. *J. Am. Chem. Soc.* **1998**, *120*, 1581–1587. (i) Yoshida, T.; Koga, N.; Morokuma, K. *Organometallics* **1996**, *15*, 766–777. (j) Margl, P.; Deng, L.; Ziegler, T. *Organometallics* **1998**, *17*, 933–946. (k) Deng, L.; Margl, P.; Ziegler, T. *J. Am. Chem. Soc.* **1997**, *119*, 1094–1100. (l) Tobisch, S.; Bogel, H.; Taube, R. *Organometallics* **1998**, *17*, 1177–1196. (m) Tobisch, S. *J. Am. Chem. Soc.* **2004**, *126*, 259–272. (n) Lanza, G.; Fragala, I. L.; Marks, T. J. *Organometallics* **2001**, *20*, 4006–4017. (o) Lanza, G.; Fragala, I. L.; Marks, T. J.

- Organometallics* **2002**, *21*, 5594–5612. (p) Novaro, O.; Blaisten-Baroja, E.; Clementi, E.; Giunchi, G.; Ruiz-Vizcaya, M. E. *J. Chem. Phys.* **1978**, *68*, 2337–2351. (q) Fujimoto, H.; Yamasaki, T.; Mizutani, H.; Koga, N. *J. Am. Chem. Soc.* **1985**, *107*, 6157–6161. (r) Kawamura-Kurabayashi, H.; Koga, N.; Morokuma, K. *J. Am. Chem. Soc.* **1992**, *114*, 2359–2366. (s) Koga, N.; Yoshida, T.; Morokuma, K. *Organometallics* **1993**, *12*, 2777–2787. (t) Weiss, H.; Ehrig, M.; Ahlrichs, R. *J. Am. Chem. Soc.* **1994**, *116*, 4919–4928. (u) Bierwagen, E. P.; Bercaw, J. E.; Goddard, W. A. *J. Am. Chem. Soc.* **1994**, *116*, 1481–1489. (v) Linnolahti, M.; Pakkanen, T. A. *Macromolecules* **2000**, *33*, 9205–9214. (w) Motta, A.; Fragala, I. L.; Marks, T. *J. Am. Chem. Soc.* **2008**, *130*, 16533–16546. (x) Yang, S. Y.; Ziegler, T. *Organometallics* **2006**, *25*, 887–900. (y) Guerra, G.; Corradini, P.; Cavallo, L. *Macromolecules* **2005**, *38*, 3973–3976. (z) Zhang, Y.; Ning, Y.; Caporaso, L.; Cavallo, L.; Chen, E. Y. X. *J. Am. Chem. Soc.* **2010**, *132*, 2695–2709.
- (10) (a) Michalak, A.; Ziegler, T. *Organometallics* **1999**, *18*, 3998–4004. (b) Michalak, A.; Ziegler, T. *J. Am. Chem. Soc.* **2002**, *124*, 7519–7528. (c) Michalak, A.; Ziegler, T. *Kinet. Catal.* **2006**, *47*, 310–325. (d) Liu, Y.; Zhang, M.; Drew, M. G. B.; Yang, Z.; Liu, Y. *J. Mol. Struct.: THEOCHEM* **2005**, *726*, 277–283. (e) Yang, Z.; Liu, Y.; Liu, Y. *Chinese J. Struct. Chem.* **2005**, *24*, 723–728. (f) Liu, Y.; Liu, Y.; Drew, M. G. B. *Struct. Chem.* **2010**, *21*, 21–28. (g) Moscardi, G.; Resconi, L. *Organometallics* **2001**, *20*, 1918–1931. (h) Mitani, M.; Furuyama, R.; Mohri, J.; Saito, J.; Ishii, S.; Terao, H.; Nakano, T.; Tanaka, H.; Fujita, T. *J. Am. Chem. Soc.* **2003**, *125*, 4293–4305. (i) Borrelli, M.; Busico, V.; Cipullo, R.; Ronca, S. *Macromolecules* **2003**, *36*, 8171–8177. (j) Saßmannshausen, J. *Dalton Trans.* **2009**, 8993–8999. (k) Lee, J. W.; Jo, W. H. *J. Organomet. Chem.* **2009**, *694*, 3076–3083. (l) Caporaso, L.; Rosa, C. D.; Talarico, G. *J. Polym. Sci., Part A: Polym. Chem.* **2010**, *48*, 699–708.
- (11) (a) Kirillov, E.; Lavanant, L.; Thomas, C.; Roisnel, T.; Chi, Y.; Carpentier, J. F. *Chem.—Eur. J.* **2007**, *13*, 923–935. (b) Landis, C. R.; Rosaen, K. A.; Uddin, J. *J. Am. Chem. Soc.* **2002**, *124*, 12062–12063. (c) Zuccaccia, C.; Busico, V.; Cipullo, R.; Talarico, G.; Froese, R. D. J.; Vosejpk, P. C.; Hustad, P. D.; Macchioni, A. *Organometallics* **2009**, *28*, 5445–5458. (d) Manz, T. A.; Sharma, S.; Phomphrai, K.; Novstrup, K. A.; Fenwick, A. E.; Fanwick, P. E.; Medvedev, G. A.; Abu-Omar, M. M.; Delgass, W. N.; Thomson, K. T.; Caruthers, J. M. *Organometallics* **2008**, *27*, 5504–5520. (e) Manz, T. A.; Phomphrai, K.; Sharma, G. S.; Haq, J.; Novstrup, K. A.; Thomson, K. T.; Delgass, W. N.; Caruthers, J. M.; Abu-Omar, M. M. *J. Am. Chem. Soc.* **2007**, *129*, 3776–3777.
- (12) (a) Tredget, C. S.; Clot, E.; Mountford, P. *Organometallics* **2008**, *27*, 3458–3473. (b) Zhang, L.; Suzuki, T.; Luo, Y.; Nishiura, M.; Hou, Z. *Angew. Chem., Int. Ed.* **2007**, *46*, 1909–1913. (c) Li, X.; Nishiura, M.; Hu, L.; Mori, K.; Hou, Z. *J. Am. Chem. Soc.* **2009**, *131*, 13870–13882. (d) Zhang, L.; Luo, Y.; Hou, Z. *J. Am. Chem. Soc.* **2005**, *127*, 14562–14563. (e) Luo, Y.; Hou, Z. *Organometallics* **2006**, *25*, 6162–6165. (f) Luo, Y.; Luo, Y.; Qu, J.; Hou, Z. *Organometallics* **2011**, *30*, 2908–2919. (g) Du, G.; Wei, Y.; Ai, L.; Chen, Y.; Xu, Q.; Liu, X.; Zhang, S.; Hou, Z.; Li, X. *Organometallics* **2011**, *30*, 160–170. (h) Liu, J.; Ling, J.; Shen, Z. *J. Mol. Cat. A Chem.* **2009**, *300*, 59–64. (i) Paoluccia, G.; Bortoluzzi, M.; Napolib, M.; Longob, P.; Bertolasic, V. *J. Mol. Cat. A Chem.* **2010**, *317*, 54–60. (j) Ling, J.; Shen, J.; Hogen-Esch, T. E. *Polymer* **2009**, *50*, 3575–3581. (k) Perrin, L.; Bonnet, F.; Visseaux, M.; Maron, L. *Chem. Commun.* **2010**, *46*, 2965–2967. (l) Perrin, L.; Sarazin, Y.; Kirillov, E.; Carpentier, J. F.; Maron, L. *Chem.—Eur. J.* **2009**, *15*, 3773–3783. (m) Perrin, L.; Bonnet, F.; Chenal, T.; Visseaux, M.; Maron, L. *Chem.—Eur. J.* **2010**, *16*, 11376–11385. (n) Perrin, L.; Kirillov, E.; Carpentier, J. F.; Maron, L. *Macromolecules* **2010**, *43*, 6330–6336. (o) Annunziata, L.; Rodrigues, A. S.; Kirillov, E.; Sarazin, Y.; Okuda, J.; Perrin, L.; Maron, L.; Carpentier, J. F. *Macromolecules* **2011**, *44*, 3312–3322.
- (13) Selected examples: (a) Luo, Y.; Selvam, P.; Endou, A.; Kubo, M.; Miyamoto, A. *J. Am. Chem. Soc.* **2003**, *125*, 16210–16212. (b) Luo, Y.; Selvam, P.; Ito, Y.; Takami, S.; Kubo, M.; Imamura, A.; Miyamoto, A. *Organometallics* **2003**, *22*, 2181–2183. (c) Luo, Y.; Baldamus, J.; Tardif, O.; Hou, Z. *Organometallics* **2005**, *24*, 4362–4366. (d) Luo, Y.; Hou, Z. *Organometallics* **2007**, *26*, 2941–2944.
- (e) Luo, Y.; Hou, Z. *Int. J. Quantum Chem.* **2007**, *107*, 374–381. (f) Luo, Y.; Hou, Z. *J. Phys. Chem. C* **2008**, *112*, 635–638.
- (14) (a) Svensson, M.; Humbel, S.; Froese, R. D. J.; Matsubara, T.; Sieber, S.; Morokuma, K. *J. Phys. Chem.* **1996**, *100*, 19357–19363. (b) Maseras, F.; Morokuma, K. *J. Comput. Chem.* **1995**, *16*, 1170–1179. (c) Vreven, T.; Morokuma, K. *J. Comput. Chem.* **2000**, *21*, 1419–1432.
- (15) Frisch, M. J.; Trucks, G. W.; Schlegel, H. B.; Scuseria, G. E.; Robb, M. A.; Cheeseman, J. R.; Scalmani, G.; Barone, V.; Mennucci, B.; Petersson, G. A.; Nakatsuji, H.; Caricato, M.; Li, X.; Hratchian, H. P.; Izmaylov, A. F.; Bloino, J.; Zheng, G.; Sonnenberg, J. L.; Hada, M.; Ehara, M.; Toyota, K.; Fukuda, R.; Hasegawa, J.; Ishida, M.; Nakajima, T.; Honda, Y.; Kitao, O.; Nakai, H.; Vreven, T.; Montgomery, J. A.; Jr.; Peralta, J. E.; Ogliaro, F.; Bearpark, M.; Heyd, J. J.; Brothers, E.; Kudin, K. N.; Staroverov, V. N.; Kobayashi, R.; Normand, J.; Raghavachari, K.; Rendell, A.; Burant, J. C.; Iyengar, S. S.; Tomasi, J.; Cossi, M.; Rega, N.; Millam, J. M.; Klene, M.; Knox, J. E.; Cross, J. B.; Bakken, V.; Adamo, C.; Jaramillo, J.; Gomperts, R.; Stratmann, R. E.; Yazeyev, O.; Austin, A. J.; Cammi, R.; Pomelli, C.; Ochterski, J. W.; Martin, R. L.; Morokuma, K.; Zakrzewski, V. G.; Voth, G. A.; Salvador, P.; Dannenberg, J. J.; Dapprich, S.; Daniels, A. D.; Farkas, O.; Foresman, J. B.; Ortiz, J. V.; Cioslowski, J.; Fox, D. J. *Gaussian 09, Revision A.02; Gaussian, Inc.: Wallingford CT*, 2009.
- (16) Rappé, A. K.; Casewit, C. J.; Colwell, K. S.; Goddard, W. A. III; Skiff, W. M. *J. Am. Chem. Soc.* **1992**, *114*, 10024–10035.
- (17) (a) Dolg, M.; Wedig, U.; Stoll, H.; Preuss, H. *J. Chem. Phys.* **1987**, *86*, 866–872. (b) Schwerdtfeger, P.; Dolg, M.; Schwarz, W. H. E.; Bowmaker, G. A.; Boyd, P. D. W. *J. Chem. Phys.* **1989**, *91*, 1762–1774. (c) Dolg, M.; Stoll, H.; Savin, A.; Preuss, H. *Theor. Chim. Acta* **1989**, *75*, 173–194. (d) Andrae, D.; Haeussermann, U.; Dolg, M.; Stoll, H.; Preuss, H. *Theor. Chim. Acta* **1990**, *77*, 123–141. (e) Dolg, M.; Stoll, H.; Preuss, H. *Theor. Chim. Acta* **1993**, *85*, 441–450. (f) Bergner, A.; Dolg, M.; Kuechle, W.; Stoll, H.; Preuss, H. *Mol. Phys.* **1993**, *80*, 1431–1441.
- (18) (a) Cossée, P. *J. Catal.* **1964**, *3*, 80–88. (b) Arlman, E. J. *J. Catal.* **1964**, *3*, 89–98. (c) Arlman, E. J.; Cossée, P. *J. Catal.* **1964**, *3*, 99–104. (d) Brookhart, M.; Green, M. L. H. *J. Organomet. Chem.* **1983**, *250*, 395–408. (e) Grubbs, R.; Coates, G. W. *Acc. Chem. Res.* **1996**, *29*, 85–93. (f) Fan, L.; Harrison, D.; Woo, T. K.; Ziegler, T. *Organometallics* **1995**, *14*, 2018–2026.
- (19) Resconi, L.; Cavallo, L.; Fait, A.; Piemontesi, F. *Chem. Rev.* **2000**, *100*, 1253–1345.
- (20) Lynch, B. J.; Truhlar, D. G. *J. Phys. Chem. A* **2003**, *107*, 3898–3906.